Article

Exploring the Programmable Assembly of a Polyoxometalate-Organic Hybrid via Metal Ion Coordination

Panchao Yin, Tao Li, Ross S. Forgan, Claire Lydon, Xiaobing Zuo, Zhaoxiong Norm Zheng, Byeongdu Lee, De-Liang Long, Leroy Cronin, and Tianbo Liu

J. Am. Chem. Soc., **Just Accepted Manuscript** • DOI: 10.1021/ja404777g • Publication Date (Web): 09 Aug 2013

Exploring the Programmable Assembly of a Polyoxometalate-Organic Hybrid via Metal Ion Coordination

Panchao Yin,[†] Tao Li,[‡] Ross S. Forgan,[¶] Claire Lydon,[¶] Xiaobing Zuo,[‡] Zhaoxiong Norm Zheng,[†] Byeongdu Lee,[‡] Deliang Long, [¶] Leroy Cronin,*[,¶] and Tianbo Liu*[,†,±]

[†]Department of Chemistry, Lehigh University, Bethlehem, PA 18015, USA

[‡]X-ray Science Division, Advanced Photo Source, Argonne National Laboratory, Argonne, IL 60439, USA

[¶]WestCHEM, School of Chemistry, University of Glasgow, Glasgow, G12 8QQ, UK

[±]Department of Polymer Science, The University of Akron, Akron, OH 44325, USA

*The correspondence should be addressed.

ABSTRACT: The conformational flexibility and programmed assembly of a dumbbell-shaped polyoxometalate-organic hybrid molecule comprising two Dawson-type polyoxometalates linked by a 2,2'-bipyridine unit which can be coordinate to metal ions, in this case of Zn^{2+}, is described. SAXS, UV/Vis, and NMR spectroscopic techniques confirm that the hybrid molecules exist as the *trans* dumbbell in metal-ion-free solutions, and can be reversibly transformed into the *cis* dumbbell through coordination upon the addition of $ZnCl_2$ into a DMSO solution containing the hybrid. Subsequent addition of EDTA reverses the switching process by extracting the Zn^{2+} cations from the hybrid. During the interchange process between *trans* and *cis* dumbbells, a

further reorganization of the hybrid molecules occurs through bond rotation to minimize steric clashes between the polyoxometalate subunits, in order to stabilize the corresponding dumbbell conformation. The Zn^{2+}-controlled conformational transformation of the hybrid can be further utilized to manipulate the hybrid's solvophobic interaction-driven self-assembly behavior in the metal-ion driven reversible formation of 140 nm sized vesicles, studied by laser light scattering techniques.

INTRODUCTION

Molecular switches are molecules that can be reversibly shifted between two or more stable states in response to environmental stimuli, e.g. pH, light, temperature, redox potential, electric field, and the presence of ligands or metal ions.[1-14] In particular, the control of supramolecular assembly *via* metal ion coordination is a very useful approach to preparing artificial molecular switches,[13,15,16] and is vital in many biological behaviors, e.g. metal ion-directed protein folding and self-assembly, Ca^{2+} induced contraction or relaxation of the human heart, Na^{+} stimulated nerve impulses, and the Ca^{2+}-gated K^{+} ion channel found inside cell membranes.[17-20] It remains challenging, however, to build artificial metal-ion-driven molecular switches based on relatively simple molecules that operate on the tens of kDa scale of proteins and demonstrate significant modification of self-assembly behavior. Molecular switches that respond to metal ion stimuli can suffer from the fact that complexation often only affects significantly the local area around the metal binding site, limiting the functionality of the switches. Moreover, molecular switches that display metal-ion-responsive folding and self-assembly behavior could be thought of as simple models to help us understand the corresponding biological process involving proteins and RNAs.

Polyoxometalates (POMs) are a large group of structurally well-defined molecular metal-oxide clusters (*ca.* 1 ~ 6 nm) with diverse physical properties and applications.[21-24] Chemically grafting organic ligands/chains onto the POMs results in POM-organic hybrids, which can maintain, modify, or enhance the optical,[25-27] electrical,[28,29] thermal,[30] and fluorescence[31-33] properties of the POMs. The functionality (e.g. self-assembly behavior and catalytic activity) of POM-based hybrids relies significantly on their molecular conformation and, therefore, POMs which exhibit conformational changes in response to external stimuli could be used as 'switches' to enhance or remove these functions. Herein, we report, to the best of our knowledge, the first example of a POM-based metal-ion-driven molecular switch, which demonstrates a reversible switching process upon the coordination of Zn^{2+} cations. Moreover, during the interchange between the *trans* and *cis* dumbbells, a further reorganization of the hybrid molecules occurs through bond rotation to minimize steric clashes between the polyoxometalate subunits, in order to stabilize the corresponding dumbbell conformation. This controllable metal ion translocation is used to reversibly tune the packing parameter of the POM-based hybrid (which can be treated as an amphiphile) and its consequent self-assembly behavior in the metal-ion driven reversible formation of 140 nm sized vesicles, as studied by laser light scattering (LLS) and TEM techniques. The working cycles of the molecular switch were also monitored by UV-vis and ^{1}H-NMR spectroscopy, and the switching process was elucidated both by Synchrotron Small-Angle X-Ray Scattering (SAXS) and 2D Nuclear Overhauser Effect Spectroscopy (NOESY).

RESULTS AND DISCUSSION

Molecular Structure of the Hybrid Molecular Switch. Hybrid **1**, $TBA_{10}H_2[\{P_2V_3W_{15}O_{59}(OCH_2)_3CNHCO\}_2(C_5H_3N)_2]$ (TBA, tetrabutylammonium), has been reported and fully characterized in a previous publication.[34] The hybrid has a dumbbell-like shape with the two Dawson-type POMs at opposite ends linked by a 2,2'-bipyridine unit, as evidenced by the crystal structure of a partially cation-exchanged sample (see experimental section for details) displayed in Figure 1. The covalent but non-conjugated linkage between the organic and inorganic building blocks of **1** ensures the molecule is quite stable whilst the functionalities of different components are maintained. The size of the molecule is *ca.* $1 \times 1 \times 4$ nm^3 and it has a molecular weight of *ca.* 10.6 kDa. The 2,2'-bipyridine unit has been explored with respect to the incorporation into the design of switchable molecules because of the metal-ion-induced conformational rotation around the central C-C single bond which occurs upon coordination of the metal ion.[35-38] The purpose of designing hybrid **1** is to transfer the metal-ion-responsive behavior from the bipyridine unit to the hybrid POMs, study the interaction between the highly charged and bulky POM units in *trans*- and *cis*- dumbbell, and control the hydrophobicity-driven self-assembly behavior through the introduction of metal ions. The POM units are connected to the 4, 4' positions of the heteroaromatic rings, which not only can extend the bipyridine unit's conformation change to the entire hybrid molecule, but also attenuate somewhat the possible steric hindrance between the two POM units during the rotation process (Figure 2). Based on the above assumption, the hybrid can exist in two conformations: the *trans* dumbbell in a metal-ion-free environment, as illustrated in the solid-state structure, and the *cis* dumbbell driven by the coordination of the two nitrogen atoms of the central 2,2'-bipy unit to a metal ion.

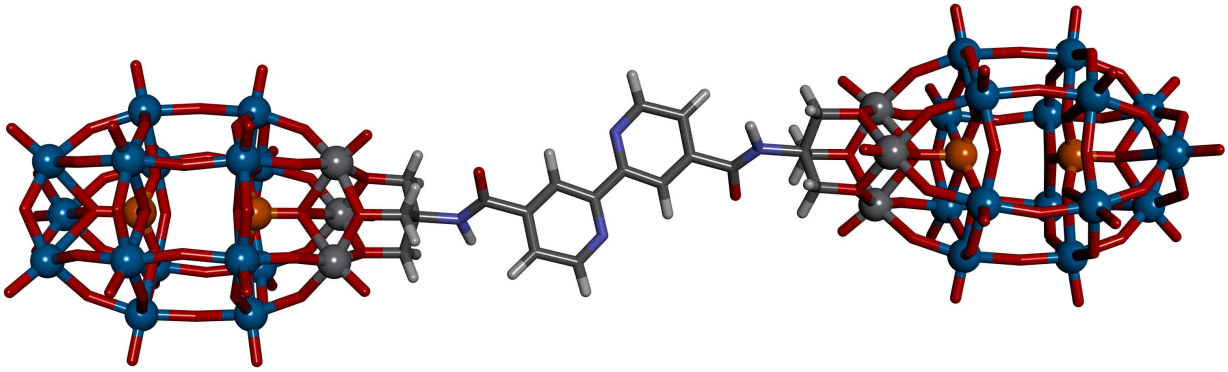

Figure 1. Representation of the molecular structure of the anionic component of hybrid **1**. Counterions and solvent molecules have been removed for clarity. Color code: W-blue, V-grey, P-orange spheres; C-grey, O-red, N-blue, H-white sticks.

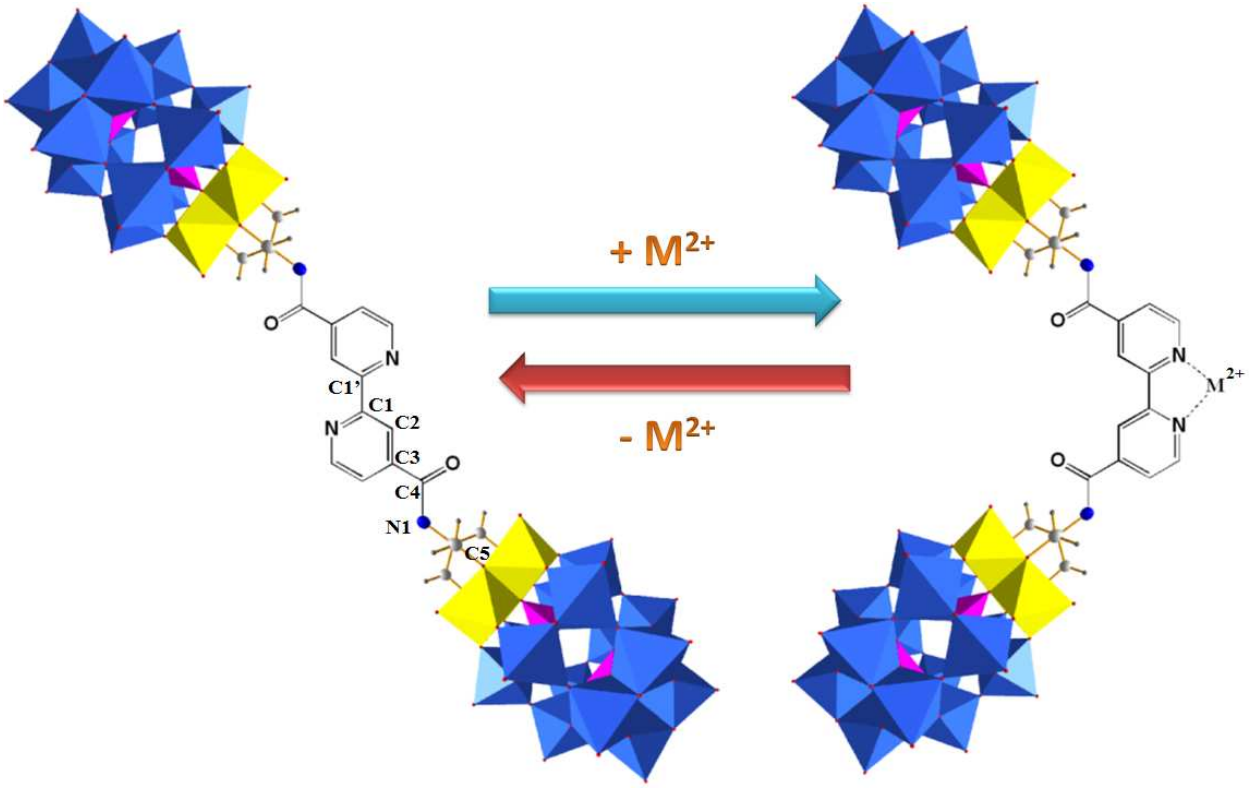

Figure 2. The reversible conformational transformation that occurs when **1** (denoted the *trans* dumbbell herein) is complexed by a divalent metal chloride to form the complexed (*cis*) dumbbell.

UV/vis Monitoring the *Trans* to *Cis* Dumbbell Transformation Process. Titration of $ZnCl_2$ into a DMSO solution of the pure bipyridine ligand without POM attachments results in a classical bathochromic shift of the bipyridine-based absorption from λ_{max} of *ca.* 300 to 330 nm, which is attributed to the complexation between Zn^{2+} ions and the ligand (Figures S1 and S2 in supporting information). A resolved absorption peak for the bipyridine moiety is not observed in the UV/vis spectrum of hybrid **1**, because the strong absorption peak of the Dawson-type POM unit obscures it. Despite this, a similar bathochromic shift can be observed when Zn^{2+} is added to a DMSO solution of **1** (Figure 3). For a control titration experiment, $ZnCl_2$ is titrated against the dumbbell-shaped hybrid **2**[39] which has an oxalate-based linker rather than a bipyridine one (Figure S3 and S4 in supporting information). It induces no obvious change in the UV/vis spectrum, ruling out the possibility that the interaction between the anionic POM subunit and Zn^{2+} ions contributes to the bathochromic shift. As a result, the addition of Zn^{2+} is expected to trigger the formation of a Zn-bipyridine complex and consequently change the conformation of the dumbbell structure from *trans* to *cis*.

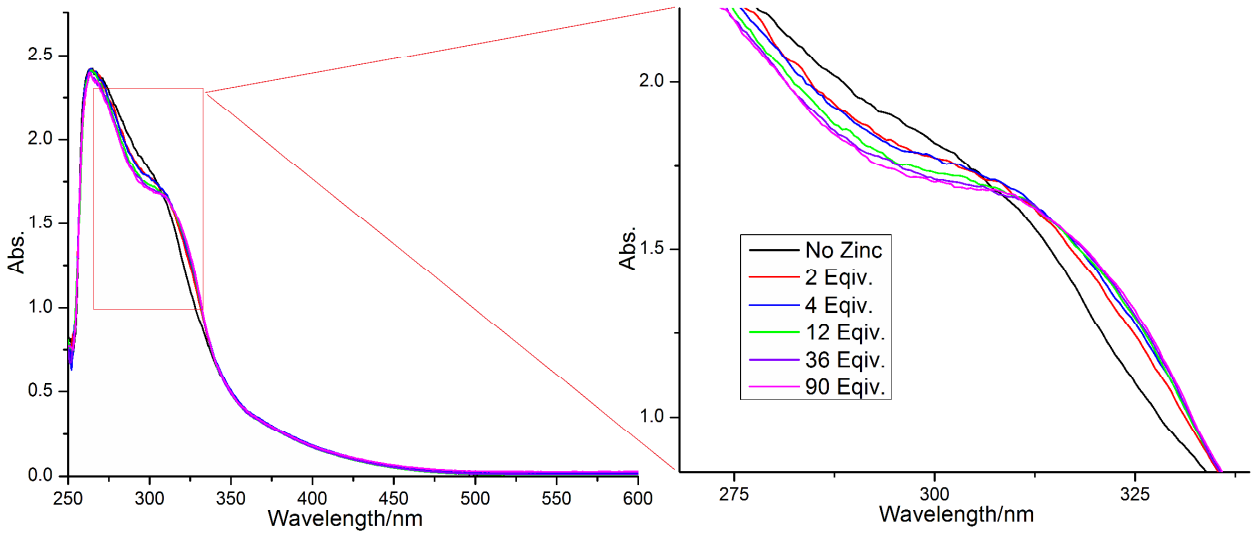

Figure 3. UV-Vis monitoring of the titration of $ZnCl_2$ into a DMSO solution of hybrid **1**.

^{1}H-NMR Monitoring of the Reversible Transformation Process. ^{1}H-NMR spectroscopy was used to obtain detailed information regarding the reversibility of the metal-ion-driven switching process. ^{1}H-NMR spectroscopic studies in DMSO-d_6 on the bipyridine ligand without POM attachments shows downfield shifts and broadening of the resonances associated with the heteroaromatic rings and amino groups in the spectrum of the ligand upon the addition of $ZnCl_2$. The signal changes reach a maximum after the Zn^{2+} ions reach a molar ratio of 3.5:1 to bipyridine (i.e., 3.5 equivalents, see Figure S5). This peak shifting and broadening effect is characteristic of complexation. A similar phenomenon can be observed in the corresponding experiments (Figure 4) with hybrid **1**. After titrating larger amounts of $ZnCl_2$ into the hybrid solution (up to 40 equivalents), the signals corresponding to H*a* and H*c* at 7.85 and 8.75 ppm, respectively, gradually decrease, coinciding with the appearance and growth of two new peaks at 8.15 and 9.05 ppm, indicating the Zn^{2+}-complexation controlled *trans* to *cis* transformation. Meanwhile, the peaks assigned to H*b* and H*d*, at 8.45 and 8.85 ppm, respectively, continuously move downfield to 8.55 and 8.90 ppm, respectively. As high as *ca.* 40 equivalents of $ZnCl_2$ are needed to fully convert the *trans* dumbbell of hybrid **1** to the *cis* dumbbell, probably due to the repulsive interaction between the giant Dawson clusters during the rotation process. Interestingly, the downfield shifted peaks return to their original upfield positions after the addition of *ca.* 20 equivalents of $(TBA)_4$·EDTA (tetra-*n*-butylammonium ethylenediaminetetraacetate, see experimental section), suggesting that the EDTA chelates the Zn^{2+} ions by extracting them from the *cis* dumbbell, which subsequently converts by rotation around the C–C bond to the *trans* dumbbell configuration. The addition of Zn^{2+} ions and their later removal with EDTA in the DMSO solution of hybrid **1** can be considered as a running cycle of a molecular switch (Figure 2). Further ^{1}H-NMR studies confirm that the Zn^{2+}-controlled

switching process occurs seamlessly for at least 5 cycles without decomposition of the hybrids or dysfunctionality (Figure S7 in support information).

Additionally, the *trans* to *cis* dumbbell transformation leads to an observable change in the diffusion speed of the hybrid molecule, as measured by 2D diffusion ordered ^{1}H NMR spectroscopy (DOSY). The DOSY results divulge diffusion coefficients (D) of 7.9 x 10^{-11} m^2s^{-1} for the *trans* dumbbell (before adding $ZnCl_2$) and 1.3 x 10^{-10} m^2s^{-1} for the *cis* dumbbell. Based on the Stokes-Einstein diffusion equation (Equation provided in experimental section), the hydrodynamic radii (R_h) of the *trans* dumbbell and the *cis* dumbbell can be calculated as 1.4 nm and 0.8 nm, respectively. This observation could be explained by the shorter distance between two Dawson-type POMs in the *cis* dumbbell than in the *trans* dumbbell.

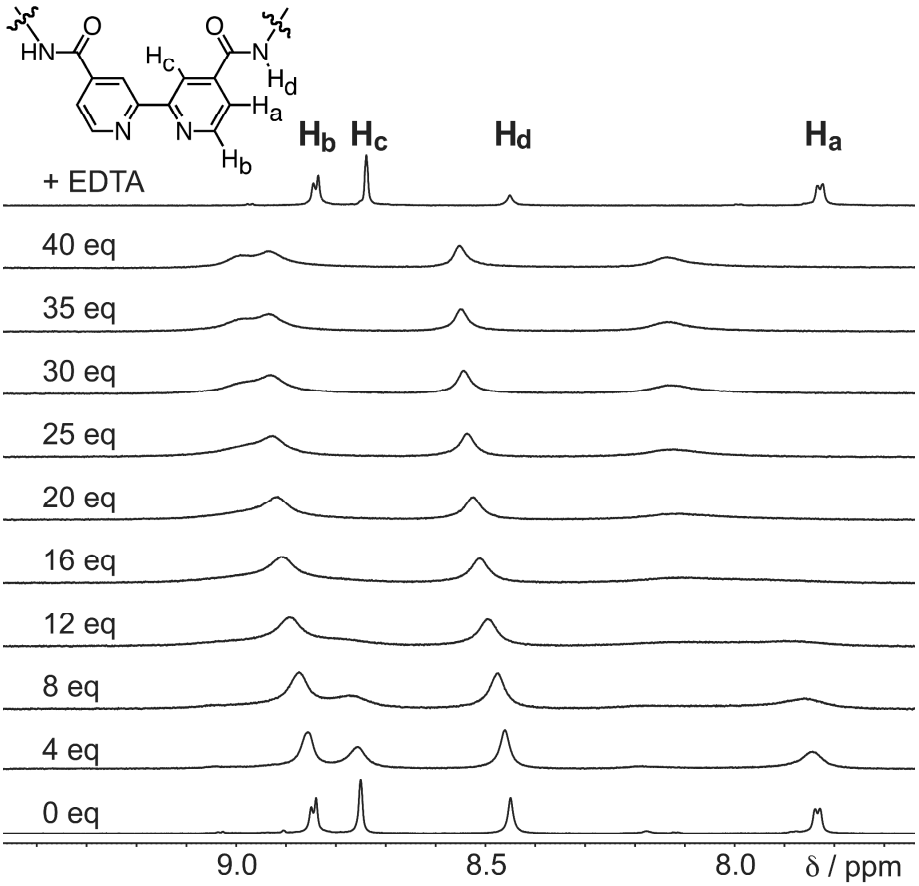

Figure 4. Stacked partial ^{1}H-NMR spectra (500 MHz, DMSO-d_6, 298 K) covering the addition of 0-40 equivalents of $ZnCl_2$ to 25 mg of the hybrid **1** dissolved in DMSO-d_6, showing signal broadening and shifting upon complexation of the Zn^{2+} to the bipyridine unit. The spectrum of the sample after subsequent addition of $(TBA)_4$·EDTA (top) which chelates the Zn^{2+} cations shows signals commensurate with the metal-free hybrid. The assignment of the resonances in **1** was confirmed by a ^{1}H-^{1}H COSY spectrum (see supporting information).

Observation of Coordination Driven Switch by SAXS and NOESY. The molecular framework of hybrid **1** is essentially rigid and only five single bonds are allowed to rotate (the pair of C4-N1, the pair of C3-C4, and C1-C1′ in Figure 1 and 2); these bonds control the molecular conformation. However, due to the symmetrical structure of the Dawson-type POM, rotation of the pair of C5-N1 single bonds has no effect on changing the hybrid's conformation. The rotation of C1-C1′ bond, and thus the *cis*-*trans* switch, highly relies on the complexation of the bipyridine chelating unit with metal ions. In addition, the C3-C4 bond is critical for the study of the co-conformation of both the *trans* and the *cis* dumbbells. Our experimental results and the consideration of minimized energy of the dumbbell structure suggest that the amide groups and the neighboring heteroaromatic rings are expected to adopt a co-planar orientation because of the conjugative effect, which will limit the possible co-conformations for both the *cis* dumbbell and the *trans* dumbbell to only 3 each (Figure 1, Figure 5, and discussions in supporting information). SAXS, a powerful technique for characterizing nanostructures in solution, was used to determine the co-conformation of hybrid **1** in DMSO solution.[40-44] The SAXS profiles of hybrid **1** before (open square) and after (open circle) adding $ZnCl_2$ (Figure 6) are remarkably different, exhibiting peak maxima at q = 0.27, and 0.33 $Å^{-1}$, respectively (Figure 6a). Furthermore, the pair distance distribution functions (PDDF) in real space, p(r), were obtained using the program GNOM[45] as

shown in Figure 6b. All PDDFs exhibit a dumbbell-type bimodal feature, where the first peak describes the *intra*-subunit (Dawson-type POM) distances and is the same for both dumbbells, while the second peak describes the *inter*-subunit pair distances. The position of the second peak roughly measures the center to center distance of the two POM subunits of the dumbbell-shaped hybrid.[46] The second peak maximum is shifted from 28.5 Å to 21.2 Å after adding $ZnCl_2$, as a result of the metal-binding induced *trans* to *cis* switch; the POM subunit separation is considerably shorter in the *cis* dumbbell. In order to further probe the solution co-conformations, the theoretical PDDF for each co-conformation was calculated using the program SolX[47,48] and superimposed upon the experimental PDDFs in Figure 6c. All the three *trans* co-conformations fit well with the experimental curve due to the similar subunit separations in each. For the *cis* dumbbell, however, the calculated PDDF for *cis*-II displays the best fit to the experimental data of the *cis* dumbbell solution, indicating that it is the most populated co-conformation, with the probable slight shoulder at ca 35 Å suggesting a small contribution from the other co-conformations is possible, i.e., the dumbbells exhibit some dynamic behavior in DMSO.

To further examine the co-conformations, 2D NOESY NMR spectroscopic measurements were employed. 2D NOESY NMR spectroscopy can identify spins undergoing cross-relaxation and measure their cross-relaxation rates.[49] The intensity of NOESY cross-peaks are dependent on the distance between protons and normally a signal is observed only if the corresponding proton-proton distance is < 5 Å.[49] As such, NOESY experiments were expected to complement the SAXS studies by determining the extent of proton-proton interactions, and the proximity of the organic fragments. The NOESY spectrum recorded at room temperature on a sample of **1** dissolved in DMSO-d_6, i.e., the *trans* dumbbell, exhibited a much stronger correlation between the amido proton (H*d*) and H*c* compared to that between H*d* and H*a*, implying that *trans*-III is

the major co-conformation of the Zn-free hybrid in solution (Figures 5 and 7a), as opposed to the *trans*-I co-conformation observed in our particular solid-state sample (Figure 1). In contrast, the NOESY spectrum of a DMSO solution of **1** with 40 equivalents of $ZnCl_2$ added to induce full complexation (i.e., to form the *cis* dumbbell) exhibits significant correlations between H*d* and *both* H*a* and H*c*. This observation appears to correlate well with the SAXS result, which suggests that *cis*-II is the major co-conformation of the *cis* dumbbell solution (Figure 5 and 7b). It should be noted that *cis*-II has reduced symmetry and, as a result, we would expect the ^{1}H-NMR spectrum to exhibit six resonances for the aromatic protons since all are heterotopic, but only three broad resonances are observed. We attribute this observation to the dynamic exchange between co-conformations, through rotation of the C3-C4 bond, which is occurring fast on the NMR timescale and giving a spectrum which is the average of all co-conformations of the *cis* dumbbells, major or minor, sampled in solution.

In theory, addition of $ZnCl_2$ to **1** to stimulate the rotation of the C1-C1′ bond would change the expected major co-conformation, *trans*-III, into *cis*-III if the C3-C4 bonds do not rotate. However, the inter-POM distance (center to center) in *cis*-III is quite short (1.2 nm) and so steric hindrance/static charge repulsion is expected to be the driving force for one of the C3-C4 bonds to rotate by 180° and relieve this unfavorable strain by increasing the distance between the Dawson POM sub-units to 2.0 nm (Figure 5, 7c and video MV1 in supporting information). This further rotation of the C3-C4 bond could explain why a large excess of Zn^{2+} is required for the transformation from the *trans* to the *cis* dumbbell.

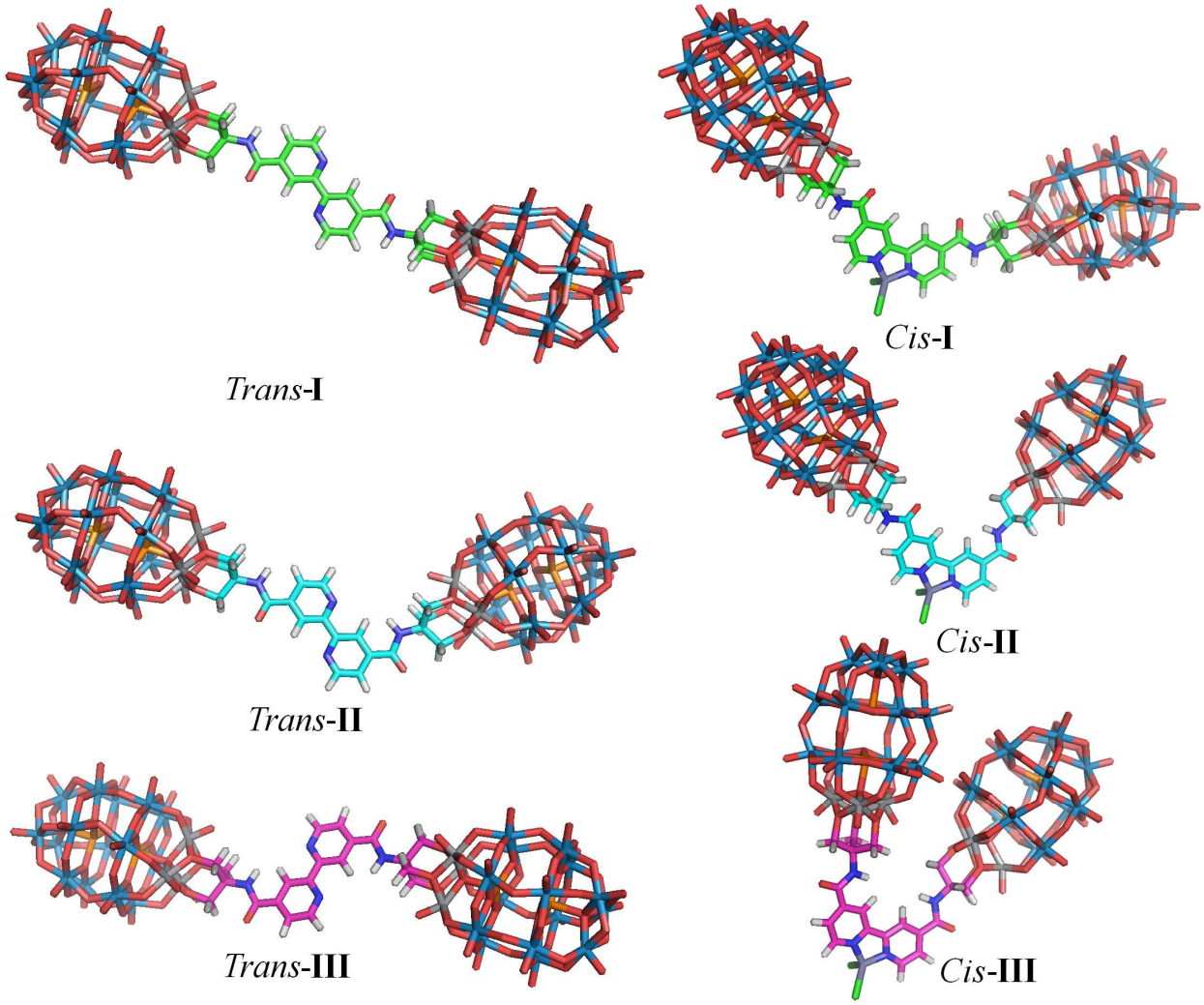

Figure 5. Calculated structures of the three possible co-conformations which can be generated by rotation around the C3-C4 bonds for both the *trans* dumbbell (Zn-free) and *cis* dumbbell (Zn complex), respectively.

SAXS was also used to confirm that the *cis* dumbbell could be converted back to the *trans* dumbbell when the Zn^{2+} ions are removed from solution by the addition of a competing chelating agent. After addition of $(TBA)_4$·EDTA, (shown in Figure 6a open triangle), the d spacing increases to around *ca.* 28 Å, based on the p(r) curve in Figure 6b (open square) indicating the hybrids have reversibly changed back again to the *trans* dumbbell, (Figure 7c).

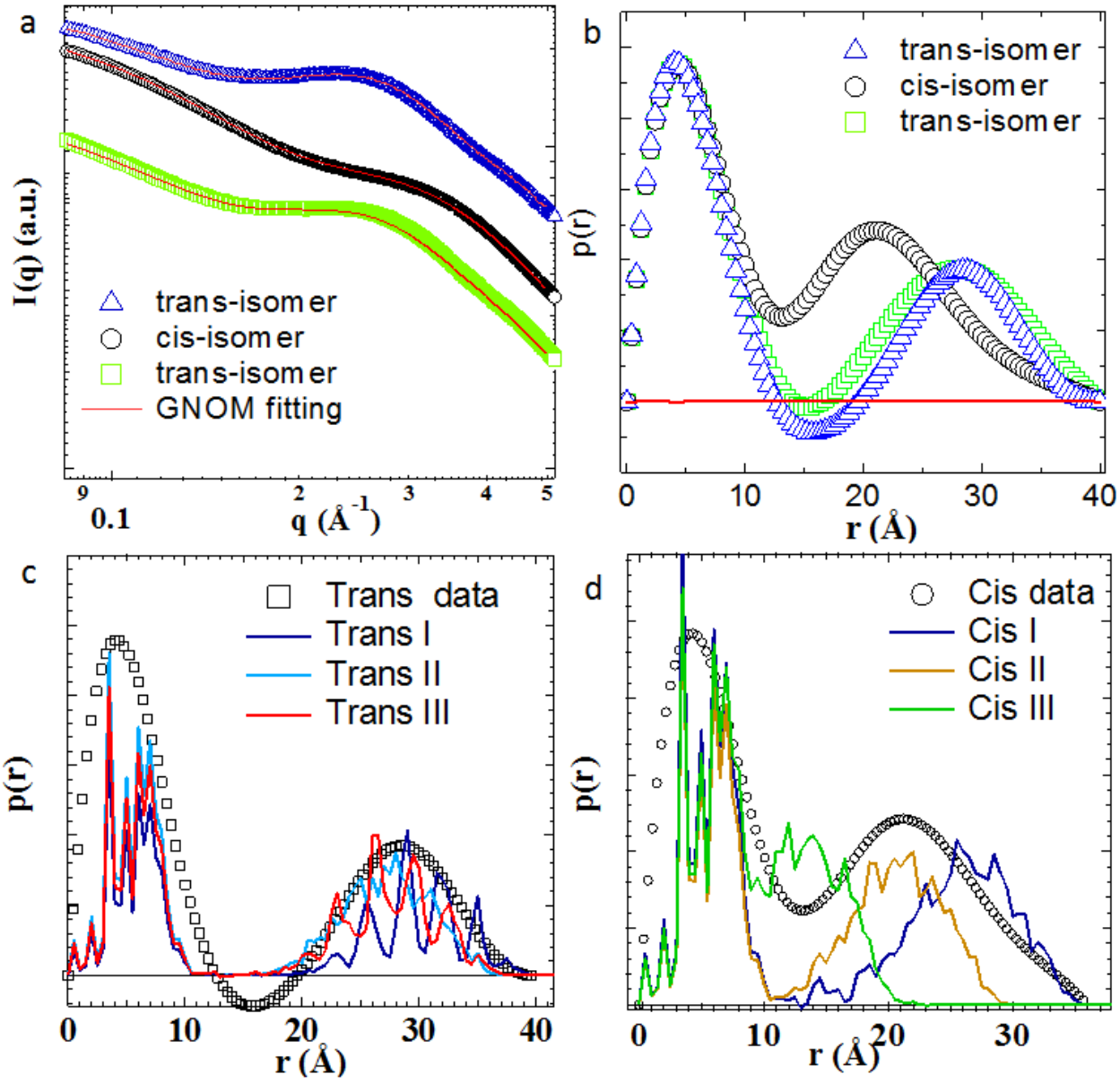

Figure 6. a) SAXS curves of DMSO solutions of the metal-free *trans* dumbbell of **1** (open squares), the *cis* dumbbell generated after adding an excess of $ZnCl_2$ (open circles), and the *trans* dumbbell which is regenerated after adding TBA_4·EDTA to the solution containing the *cis* dumbbell (open triangles). The SAXS profiles are vertically offset for clarity. b) Pair distance distribution functions (PDDFs), of the three samples obtained using the program GNOM. c) The overlay of calculated PDDFs of the three possible *trans* co-conformations and the experimentally

derived PDDF of the *trans* dumbbell. The calculated PDDFs were computed directly from the molecular coordinates using the program SolX. d) The overlay of calculated PDDFs of the three possible *cis* co-conformations and the experimental derived PDDF of the *cis* dumbbell.

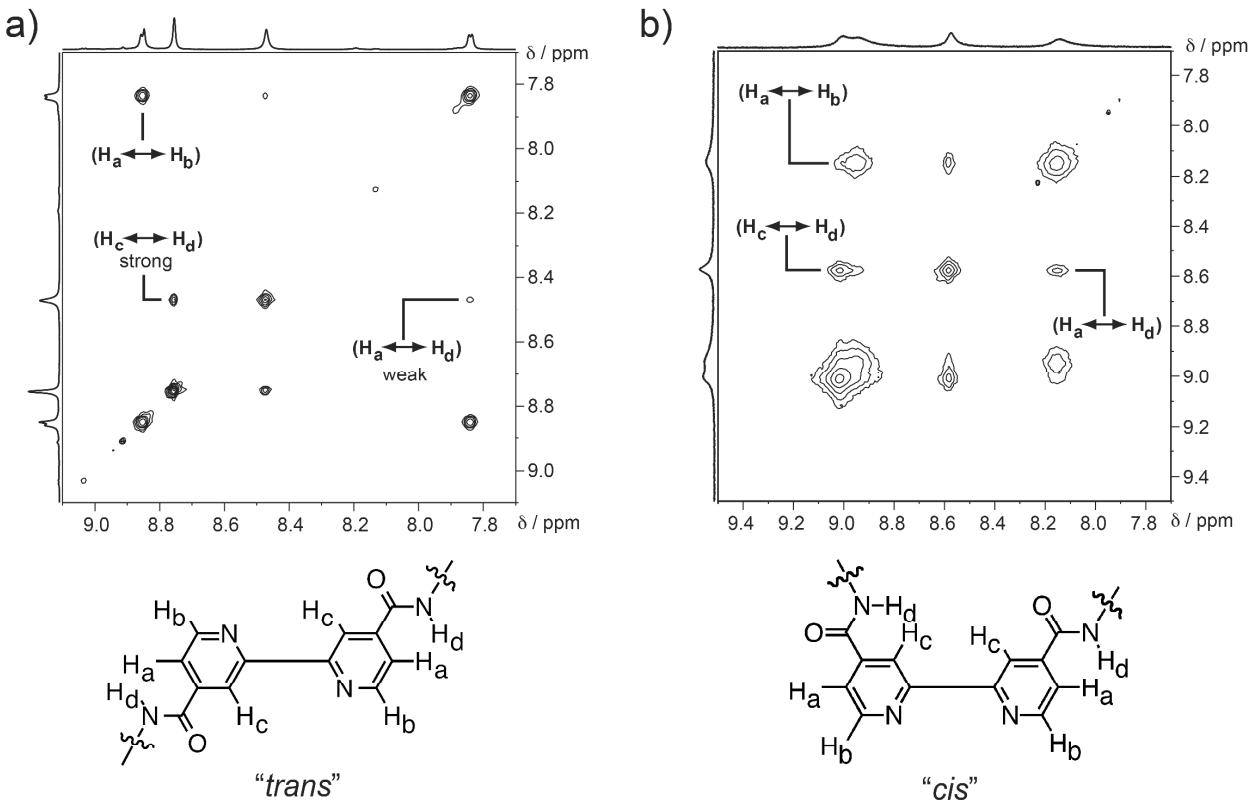

Figure 7. Labelled partial ^{1}H-^{1}H NOESY NMR spectra (500 MHz, DMSO-d_6, 298 K) of (a) hybrid **1** without Zn^{2+} and (b) hybrid **1** with 40 equivalents of $ZnCl_2$ added. The difference in relative strengths of the H*a*-H*d* and H*c*-H*d* correlation cross peaks indicate that **1** predominantly adopts the *trans*-III co-conformation and, in the presence of Zn^{2+}, the *cis*-II co-conformation, although dynamic exchange is possible. Structural diagrams for both dumbbells are given for guidance only, to show both possible orientations of the amide groups with respect to rotation around the C3-C4 bond, and the subsequent close contacts between protons.

Metal-Ion-Driven Self-Assembly/Disassembly behavior of Hybrid in Solution. It has been demonstrated previously that dumbbell-shaped hybrid POMs are amphiphilic molecules capable of forming vesicular nanostructures.[39,50,51] The self-assembly behavior of amphiphilic surfactants is controlled by various factors especially their packing parameter (*P*), which is defined as $v_o/a_e l_o$, where v_o is the surfactant tail volume, l_o is the tail length, and a_e is the equilibrium area per molecule at the aggregate surface.[52,53] In the current case, the metal-ion-driven conformational change of **1** was expected to alter its packing parameter (*P*), which might be utilized to manipulate its solvophobic-driven self-assembly behaviour. The *trans* dumbbells, when dissolved in DMSO/methanol (1:1 *v*/*v*) solution, exhibit a stable and low scattered intensity (*ca.* 40 kcps; *c.f.* scattered intensity for benzene is *ca.* 120 kcps) in time-resolved static light scattering (SLS) studies, suggesting that they exist as solvated single molecules. In contrast, the scattered intensity of this solution of **1** increased to ca. 9,000 kcps - without any precipitation - after the addition of *ca.* 18 equivalents of $ZnCl_2$, suggesting the formation of large structures. A typical CONTIN analysis from a dynamic light scattering (DLS) study on these solutions indicated the existence of assemblies with an average R_h of 138±7 nm, and with a narrow size distribution (Figure 8a), only when Zn^{2+} is present. The average radius of gyration (R_g) of these assemblies that is obtained from the SLS measurement, 144±7 nm, correlates closely with R_h, suggesting a hollow spherical vesicular structure for the assemblies. This observation is further confirmed by TEM studies (Figure 8b). By removing $ZnCl_2$ from the *cis* dumbbell through the addition of $(TBA)_4$·EDTA, the conformation of **1** should change back to *trans* and the vesicles disassemble, as indicated by the drastic drop of the scattered intensity back to 47 kcps. This controllable self-assembly and disassembly processes can be repeated with the same sample by

adding and removing $ZnCl_2$ over several cycles (TOC graph and experimental details in support information).

A control experiment using the non-functional hybrid **2** shows that no large assemblies are observed, even after 54 equivalents of Zn^{2+} ions are added (see experimental details in support information), which rules out the possibility that any POM subunit-$ZnCl_2$ interaction is the major driving force for the formation of these vesicular structures. The *trans* dumbbell of **1** is of approximately cylindrical shape with a diameter of *ca.* 1 nm; therefore the closest approach of the heteroaromatic rings in two adjacent hybrid molecules can be no less than 1 nm based on a parallel-packing model (see figure S9 in supporting information).[39,50] Since a distance of ca. 0.34 nm between the aromatic groups is necessary to form face-to-face π-π stacking contacts, it is difficult for the hydrophobic organic linker of the *trans* dumbbell to directly interact with one another due to the steric hindrance of the larger POM subunits. In a previous study, the Zn-free (i.e. *trans* dumbbell) of **1** was observed to form vesicles in highly polar solvents (water/acetone mixtures) since the alkyl tails on the TBAs are expected to strongly interact with the organic linkers in these highly polar solvents and fill the solvophobic region[39,50]. We expect that the interaction between the TBA cations and the organic linkers becomes weaker in comparatively less polar solvents, e.g. the DMSO/methanol mixtures utilized in this study, and, therefore, no assemblies of the *trans* dumbbell of **1** were observed. The *cis* dumbbell is a V-shaped molecule, with a torsion angle of 108° and a *P* value of 0.55, which is much large than that of the *trans* dumbbell, 0.40. In the proposed packing model in figure 8c, two *cis* dumbbell can strongly interact with each other through hydrophobic interactions and the π-π stacking of adjacent heteroaromatic rings, yielding inter-POM distances of > 2 nm, enabling two possible packing modes of *cis* dumbbell to form vesicles. Firstly, a monolayer structure, where two polar head

groups of **1** are located on the outer and inner surfaces, respectively, with the linkers forming the solvophobic layer of the vesicle; and secondly, a bilayer structure, where the two polar heads are on the *same* surface with the linkers residing inside the vesicle shell. The 'bent' feature of *cis*-dumbbell prefers the bilayer model of vesicles because of the easiness of packing; however, we cannot rule out the possibility of the monolayer vesicle model. The well-established theory suggests that a surfactant with packing parameter 0.5 to 1.0 is able to assemble into bilayer structures. The cis-dumbbell has a packing parameter of 0.55, therefore more likely to form bilayer vesicles.

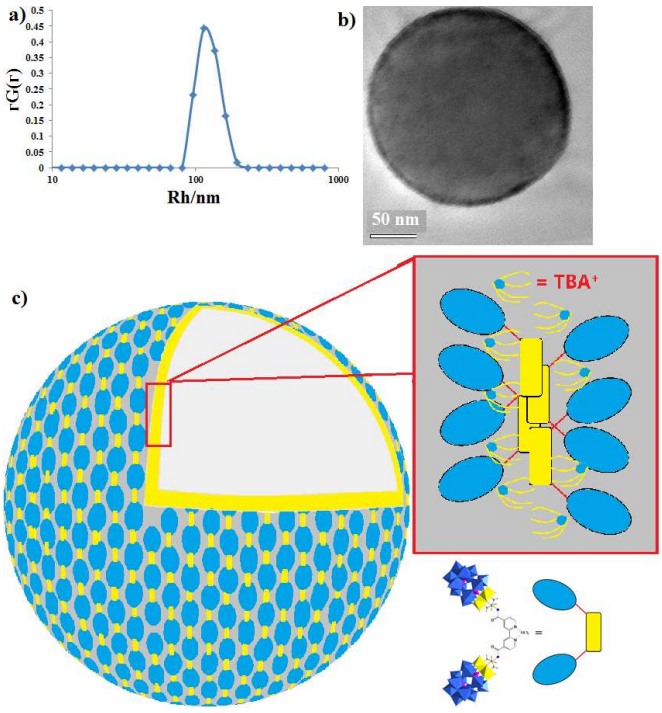

Figure 8. a) DLS results of the assemblies of Hybrid **1** in Methanol/DMSO mixed solvents at 45° scattering angle. b) TEM image of the large assembly. c) The bilayer model for the vesicle structure.

CONCLUSIONS

In summary, we have shown that the bipyridine-based dumbbell-shaped POM hybrid **1**, the first POM-based metal-ion-driven molecular switch, can be switched via the addition and removal of Zn^{2+} which in turn can dramatically change the supramolecular aggregation of the clusters. The hybrid exists as the *trans* dumbbell in metal ion-free solutions and can be converted to the *cis* dumbbell upon the coordination of zinc(II) and this is fully reversible, switching the conformation of the hybrid cluster over multiple cycles with controlled addition and removal of Zn^{2+} ions in a DMSO solution of the hybrid. A multi-responsive switching behavior is observed during the transformation process and the transformation can be further utilized to manipulate its self-assembly behavior, which is believed to mimic the behavior of metal ion-directed folding and assembly process of proteins. The current study could be helpful in not only understanding the metal ion-controlled folding and assembly behavior of biomacromolecules and designing protein-mimic smart molecules with controlled folding and self-assembly behavior, but also developing POM-based materials with tunable/modified properties (e.g. catalytic properties and encapsulation/delivery).

EXPERIMENTAL SECTION

Single Crystal X-Ray Diffraction. A sample of **1** was dissolved in dimethylformamide and subjected to partial cation exchange (TBA^+ to H^+) using Amberlite 15 cation exchange resin. Vapor diffusion of diethyl ether into the solution yielded single crystals, one of which was selected and mounted onto a rubber loop using Fomblin oil. X-Ray diffraction intensity data were collected at 150(2) K on a Bruker Apex II Quasar CCD diffractometer ($\lambda_{Mo\text{-}K\alpha}$ = 0.71073 Å) equipped with a graphite monochromator. Structure solution and refinement were carried out with SHELXS-97[54] and SHELXL-97[55] via WinGX[56] interface. The main dumbbell clusters were well defined during structure refinement but the tetrabutylammonium cations were only partially modelled with parts missing in the deep solvent area. Platon SQUEEZE[57] procedure has been

applied to the structure data to improve the structure quality and to determine the solvent void volume of crystal lattice.

Crystal data and structure refinements for $(C_{16}H_{36}N)_{10}H_2[\{P_2V_3W_{15}O_{59}(OCH_2)_3CNHCO\}_2C_{10}H_6N_2]$: $C_{180}H_{382}N_{14}O_{126}P_4V_6W_{30}$, F_w = 10704.02 g mol^{-1}; orange block crystal: 0.12 × 0.06 × 0.03 mm^3. Monoclinic, space group $P2_1/n$, a = 15.4135(5), b = 28.3495(10), c = 34.4392(12) Å, β = 93.178(2)°, V = 15025.6(9) Å^3, Z = 2, ρ = 2.366 g cm^{-3}, λ (Mo-Kα) = 0.71073, 84776 reflections measured, 23950 unique (R_{int} = 0.1054) which were used in all calculations. Final $R1$ = 0.0822 and w$R2$ = 0.2384 (all data). CCDC reference number CCDC 936592.

SAXS experimental section. The SAXS experiments were performed at 12-ID-B station with X-ray energy of 12 KeV at the Advanced Photon Source of the Argonne National Laboratory. The sample to detector distance was about 2 m. A 2D CCD detector was used to acquire images with typical exposure times in the range of 1.0 s.

TEM. The TEM images were taken on a JEOL JEM-2000 electron microscope operated at 200 kV. Samples for the TEM analysis were prepared by dropping a small volume of the solution sample onto a holey carbon film on copper grid. EDS experiments were carried out under the same condition with EDS attachments (Oxford) in JEM-2000.

Static light scattering. A commercial Brookhaven Instrument LLS spectrometer equipped with a solid-state laser operating at 532 nm was used for measurement of both SLS and DLS. SLS experiments were performed at scattering angles (θ) between 20 and 100º, at 2º intervals. However, due to the large fluctuations in scattered intensities at low scattering angles, we removed the data from 20-40º in the final analysis. Derived from Rayleigh-Gans-Debye equation[58], partial Zimm plot was used to analyze the SLS data to obtain the radius of gyration (R_g). The partial Zimm plot stems from the following approximate formula: $1/I = C(1+R_g^2*q^2/3)$. Here R_g is determined from the slope and the intercept of a plot of $1/I$ *vs.* q^2.

Dynamic light scattering. DLS measures the intensity–intensity time correlation function by means of a BI-9000AT multi-channel digital correlator. The field correlation function $|g^{(1)}(\tau)|$ was analyzed by the constrained regularized CONTIN method[59] to yield information on the distribution of the characteristic line width Γ. The normalized distribution function of the characteristic line width, G(Γ), so obtained, can be used to determine an average apparent translational diffusion coefficient, $D_{app} = \Gamma/q^2$. The hydrodynamic radius R_h is related to D via the Stokes–Einstein equation: $R_h = kT/(6\pi\eta D)$ where k is the Boltzmann constant and η the viscosity of the solvent at temperature T. From DLS measurements, we can obtain the particle-size distribution in solution from a plot of Γ*G(Γ) versus R_h. The R_h of the particles is obtained by extrapolating $R_{h,app}$ to zero scattering angle. The normalized distribution function of the characteristic line width, G(Γ), so obtained, can be used to determine an average apparent translational diffusion coefficient, $D_{app} = \Gamma/q^2$. The hydrodynamic radius R_h is related to D via the Stokes–Einstein equation: $R_h = kT/(6\pi\eta D)$ where k is the Boltzmann constant and η the viscosity of the solvent at temperature T. From DLS measurements, we can obtain the particle-size distribution in solution from a plot of Γ*G(Γ) versus R_h. The R_h of the particles is obtained by extrapolating $R_{h,app}$ to zero scattering angle.

1D NMR and 2D COSY, DOSY, and NOESY NMR Experiments. All the NMR spectra were recorded on Bruker Avance 500 MHz spectrometer equipped with a BBO probe at 298 K. 2D COSY spectra were collected under standard conditions. 2D NOESY were performed with mixing times ranging from 50 to 500 ms. The appropriate mixing time for *trans* dumbbell and *cis* dumbbell solution were determined to be 70 ms and 300 ms.

DOSY was performed on a Bruker Avance 500 MHz spectrometer with the magnetic field gradient (g) varying from 0 to 32 G/cm in 16 ~ 32 steps. The length of the gradient (d) was from 6000 ms to 8000 ms, and the time interval between two pulsedgradients (D) was from 0.1 s to 0.15 s. All spectra were taken at room temperature. After the data collection, FIDs were processed and analyzed with the NMR software TopSpin 2.0 provided by Bruker. Both T1/T2 relaxation and CONTIN methods were used to fit the raw data. The observed proton signal I in a standard DOSY spectrum is expressed through equation 1:

$$I = I_0 \exp\left[-(2\pi\gamma\delta)^2\left(\Delta - \delta/3\right)Dg^2\right] \quad \text{Equation (1)}$$

where I_0 is the reference intensity, γ is the gyromagnetic ratio of the proton. If only one diffusive component exists in the solution, a straight line will occur in a plot of $\ln(I/I_0)$ versus g^2, and the apparent diffusion coefficient (D) can be calculated from the slope using linear regression analysis.

ASSOCIATED CONTENT

Supporting Information. All experimental details, Figure S1-S11, single crystal data, and video.

This material is available free of charge via the Internet at http://pubs.acs.org.

AUTHOR INFORMATION

Corresponding Authors

*E-mail: tliu@uakron.edu (T. Liu), lee.cronin@glasgow.ac.uk (L. Cronin)

ACKNOWLEDGEMENTS

T. Liu acknowledges support from the NSF (CHE1026505), the A. P. Sloan Foundation, and Lehigh University. L. Cronin acknowledges support from EPSRC and WestCHEM. T. Li and X.

Zuo are thankful for the use of the Advanced Photon Source, an Office of Science User Facility operated for the U. S. Department of Energy (DOE) Office of Science by Argonne National Laboratory, was supported by the U.S. DOE under Contract No. DE-AC02-06CH11357.

REFERENCES

(1) Kay, E. R.; Leigh, D. A.; Zerbetto, F. *Angew. Chem. Int. Ed.* **2007**, *46*, 72.
(2) Coskun, A.; Banaszak, M.; Astumian, R. D.; Stoddart, J. F.; Grzybowski, B. A. *Chem. Soc. Rev.* **2012**, *41*, 19.
(3) Tian, H.; Yang, S. *Chem. Soc. Rev.* **2004**, *33*, 85.
(4) Saha, S.; Stoddart, J. F. *Chem. Soc. Rev.* **2007**, *36*, 77.
(5) Raymo, F. M.; Tomasulo, M. *Chem. Soc. Rev.* **2005**, *34*, 327.
(6) Tian, H.; Wang, Q.-C. *Chem. Soc. Rev.* **2006**, *35*, 361.
(7) Klajn, R.; Stoddart, J. F.; Grzybowski, B. A. *Chem. Soc. Rev.* **2010**, *39*, 2203.
(8) Otsuki, J.; Akasaka, T.; Araki, K. *Coord. Chem. Rev.* **2008**, *252*, 32.
(9) Champin, B.; Mobian, P.; Sauvage, J.-P. *Chem. Soc. Rev.* **2007**, *36*, 358.
(10) Elhabiri, M.; Albrecht-Gary, A.-M. *Coord. Chem. Rev.* **2008**, *252*, 1079.
(11) Browne, W. R.; Feringa, B. L. *Nature Nanotechnology* **2006**, *1*, 25.
(12) Feringa, B. L. *Acc. Chem. Res.* **2001**, *34*, 504.
(13) *Molecular Switches*; 2nd ed.; Feringa, B. L.; Browne, W. R., Eds.; Wiley-VCH: Weinheim, 2011; Vol. 1.
(14) Feringa, B. L.; van Delden, R. A.; Koumura, N.; Geertsema, E. M. *Chem. Rev.* **2000**, *100*, 1789.
(15) Amendola, V.; Fabbrizzi, L.; Mangano, C.; Pallavicini, P. *Acc. Chem. Res.* **2001**, *34*, 488.
(16) Fabbrizzi, L.; Licchelli, M.; Pallavicini, P. *Acc. Chem. Res.* **1999**, *32*, 846.
(17) *Metal ions in biology and medicine*; Centeno, J. A.; Collery, P.; Vernet, G.; Finkelman, R. B.; Gibb, H.; Etienne, J., Eds.; John Libbey Eurotext: Paris, France, 2000; Vol. 6.
(18) Jiang, Y.; Lee, A.; Chen, J.; Cadene, M.; Chait, B. T.; MacKinnon, R. *Nature* **2002**, *417*, 515.
(19) Salgado, E. N.; Radford, R. J.; Tezcan, F. A. *Acc. Chem. Res.* **2010**, *43*, 661.
(20) *Protein folding and metal ions : mechanisms, biology and disease*; Gomes, C. M.; Wittung-Stafshede, P., Eds.; CRC Press: Boca Raton, FL, 2011.
(21) Hill, C. L. *Chem. Rev.* **1998**, *98*, 1.
(22) Long, D.-L.; Burkholder, E.; Cronin, L. *Chem. Soc. Rev.* **2007**, *36*.
(23) Long, D.-L.; Tsunashima, R.; Cronin, L. *Angew. Chem. Int. Ed.* **2010**, *49*, 1736.
(24) Proust, A.; Thouvenot, R.; Gouzerh, P. *Chem. Commun.* **2008**, 1837.
(25) Thiel, J.; Yang, D.; Rosnes, M. H.; Liu, X.; Yvon, C.; Kelly, S. E.; Song, Y.-F.; Long, D.-L.; Cronin, L. *Angew. Chem. Int. Ed.* **2011**, *50*, 8871.
(26) Yan, Y.; Wang, H.; Li, B.; Hou, G.; Yin, Z.; Wu, L.; Yam, V. W. W. *Angew. Chem. Int. Ed.* **2010**, *49*, 9233.
(27) Yagai, S.; Ohta, K.; Gushiken, M.; Iwai, K.; Asano, A.; Seki, S.; Kikkawa, Y.; Morimoto, M.; Kitamura, A.; Karatsu, T. *Chem. Eur. J.* **2012**, *18*, 2244.

(28) Li, H.; Pang, S.; Wu, S.; Feng, X.; Müllen, K.; Bubeck, C. *J. Am. Chem. Soc.* **2011**, *133*, 9423.
(29) Yang, Y.; Xu, L.; Li, F.; Du, X.; Sun, Z. *J. Mater. Chem.* **2010**, *20*, 10835.
(30) Rieger, J.; Antoun, T.; Lee, S.-H.; Chenal, M.; Pembouong, G.; Lesage de la Haye, J.; Azcarate, I.; Hasenknopf, B.; Lacôte, E. *Chem. Eur. J.* **2012**, *18*, 3355.
(31) Yin, P.; Wu, P.; Xiao, Z.; Li, D.; Bitterlich, E.; Zhang, J.; Cheng, P.; Vezenov, D. V.; Liu, T.; Wei, Y. *Angew. Chem. Int. Ed.* **2011**, *50*, 2521.
(32) Li, D.; Song, J.; Yin, P.; Simotwo, S.; Bassler, A. J.; Aung, Y.; Roberts, J. E.; Hardcastle, K. I.; Hill, C. L.; Liu, T. *J. Am. Chem. Soc.* **2011**, *133*, 14010.
(33) Yin, P.; Jin, L.; Li, D.; Cheng, P.; Vezenov, D. V.; Bitterlich, E.; Wu, X.; Peng, Z.; Liu, T. *Chem. Eur. J.* **2012**, *18*, 6754.
(34) Pradeep, C. P.; Li, F.-Y.; Lydon, C.; Miras, H. N.; Long, D.-L.; Xu, L.; Cronin, L. *Chem. Eur. J.* **2011**, *17*, 7472.
(35) Haberhauer, G. *Angew. Chem. Int. Ed.* **2010**, *49*, 9286.
(36) Zahn, S.; Reckien, W.; Kirchner, B.; Staats, H.; Matthey, J.; Lützen, A. *Chem. Eur. J.* **2009**, *15*, 2572.
(37) Plitt, P.; Gross, D. E.; Lynch, V. M.; Sessler, J. L. *Chem. Eur. J.* **2007**, *13*, 1374.
(38) König, B.; Hollnagel, H.; Ahrens, B.; Jones, P. G. *Angew. Chem. Int. Ed.* **1995**, *34*, 2538.
(39) Pradeep, C. P.; Misdrahi, M. F.; Li, F.-Y.; Zhang, J.; Xu, L.; Long, D.-L.; Liu, T.; Cronin, L. *Angew. Chem. Int. Ed.* **2009**, *48*, 8309.
(40) Li, T.; Winans, R. E.; Lee, B. *Langmuir* **2011**, *27*, 10929.
(41) Macfarlane, R. J.; Lee, B.; Jones, M. R.; Harris, N.; Schatz, G. C.; Mirkin, C. A. *Science* **2011**, *334*, 204.
(42) Antonio, M. R.; Nyman, M.; Anderson, T. M. *Angew. Chem. Int. Ed.* **2009**, *48*, 6136.
(43) Pigga, J. M.; Kistler, M. L.; Shew, C. Y.; Antonio, M. R.; Liu, T. *Angew. Chem. Int. Ed.* **2009**, *48*, 6538.
(44) Kojima, T.; Antonio, M. R.; Ozeki, T. *J. Am. Chem. Soc.* **2011**, *133*, 7248.
(45) Svergun, D. *J. Appl. Crystallogr.* **1992**, *25*, 495.
(46) Svergun, D. I.; Koch, M. H. J. *Rep. Prog. Phys.* **2003**, *66*, 1735.
(47) Zuo, X.; Cui, G.; Merz, K. M.; Zhang, L.; Lewis, F. D.; Tiede, D. M. *Proc. Natl. Acad. Sci. USA* **2006**, *103*, 3534.
(48) Zhang, R.; Thiyagarajan, P.; Tiede, D. M. *J. Appl. Crystallogr.* **2000**, *33*, 565.
(49) Ernst, R. R.; Bodenhausen, B.; Wokaun, A. *Principles of Nuclear Magnetic Resonances in One or Two Dimesnions*; Oxford University Press: Cambridge, 1992.
(50) Misdrahi, M. F.; Wang, M.; Pradeep, C. P.; Li, F.-Y.; Lydon, C.; Xu, L.; Cronin, L.; Liu, T. *Langmuir* **2011**, *27*, 9193.
(51) Yin, P.; Li, D.; Liu, T. *Chem. Soc. Rev.* **2012**, *41*, 7368.
(52) Nagarajan, R. *Langmuir* **2001**, *18*, 31.
(53) Butt, H.-J.; Graf, K.; Kappl, M. In *Physics and Chemistry of Interfaces*; Wiley-VCH Verlag GmbH & Co. KGaA: 2004, p 246.
(54) Sheldrick, G. *Acta Crystallogr., Sect. A: Found. Crystallogr.* **1990**, *46*, 467.
(55) Sheldrick, G. *Acta Crystallogr., Sect. A: Found. Crystallogr.* **2008**, *64*, 112.
(56) Farrugia, L. *J. Appl. Crystallogr.* **1999**, *32*, 837.

(57) Sluis, P. v. d.; Spek, A. L. *Acta Crystallogr., Sect. A: Found. Crystallogr.* **1990**, *46*, 194.

(58) Hiemenz, P. C.; Rajagopalan, R. *Principles of Colloid and Surface Chemistry*; Marcel Dekker: New York, 1997.

(59) Provencher, S. W. *Comput. Phys. Commun.* **1982**, *27*, 229.

TOC

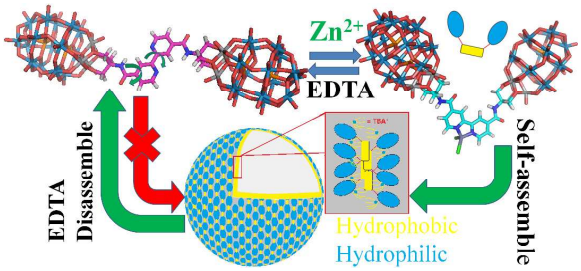
Zn2+
EDTA
EDTA
Disassemble
Self-assemble
Hydrophobic
Hydrophilic